

Highly confined surface plasmon polaritons in the ultraviolet region

E.D. CHUBCHEV,¹ I.A. NECHEPURENKO,¹ A.V. DOROFEENKO,^{1,2} A.P. VINOGRADOV,^{1,2} AND A.A. LISYANSKY,^{3,4,*}

¹Dukhov Research Institute of Automatics, 22 Suchevskaya, Moscow 120755, Russia

²Institute for Theoretical and Applied Electromagnetics of Russian Academy of Sciences, 13 Izhorskaya, Moscow 125412, Russia

³Department of Physics, Queens College of the City University of New York, Queens, NY 11367, USA

⁴The Graduate Center of the City University of New York, NY 10016, USA

*alexander.lisyansky@qc.cuny.edu

Abstract: Surface plasmon polaritons are commonly believed to be a future basis for the next generation of optoelectronic and all-optical devices. To achieve this, it is critical that the surface plasmon polariton modes be strongly confined to the surface and have a sufficiently long propagation length and a nanosize wavelength. As of today, in the visible part of the spectrum, these conditions are not satisfied for any type of surface plasmon polaritons. In this paper, we demonstrate that in the ultraviolet range, surface plasmon polaritons propagating along a periodically nanostructured aluminum-dielectric interface have all these properties. Both the confinement length and the wavelength of the mode considered are smaller than the period of the structure, which can be as small as 10 nm. At the same time, the propagation length of new surface plasmon-polaritons can reach dozens of its wavelengths. These plasmon polaritons can be observed in materials that are uncommon in plasmonics such as aluminum. The suggested modes can be used for miniaturization of optical devices.

© 2018 Optical Society of America under the terms of the [OSA Open Access Publishing Agreement](#)

OCIS codes: (250.5403) Plasmonics; (240.6680) Surface plasmons; (260.7190) Ultraviolet.

References and links

1. M. Cherchi, S. Ylino, M. Harjanne, M. Kapulainen, and T. Aalto, "Dramatic size reduction of waveguide bends on a micron-scale silicon photonic platform," *Opt. Express* **21**(15), 17814–17823 (2013).
2. S. A. Maier, *Plasmonics: Fundamentals and Applications* (Springer, 2007).
3. S. I. Bozhevolnyi, *Plasmonic Nanoguides and Circuits* (Pan Stanford, 2009).
4. D. K. Gramotnev and S. I. Bozhevolnyi, "Plasmonics beyond the diffraction limit," *Nat. Photonics* **4**(2), 83–91 (2010).
5. M. I. Stockman, "Nanoplasmonics: past, present, and glimpse into future," *Opt. Express* **19**(22), 22029–22106 (2011).
6. L. Novotny and B. Hecht, *Principles of Nano-optics* (Cambridge University, 2012).
7. E. S. Andrianov, A. P. Vinogradov, A. V. Dorofeenko, A. A. Zyablovsky, A. A. Lisyansky, and A. A. Pukhov, *Quantum Plasmonics* (Intellect, 2015).
8. R. A. Shore and A. D. Yaghjian, "Complex waves on periodic arrays of lossy and lossless permeable spheres: 1. Theory," *Radio Sci.* **47**, RS2014 (2012).
9. R. A. Shore and A. D. Yaghjian, "Complex waves on periodic arrays of lossy and lossless permeable spheres: 2. Numerical results," *Radio Sci.* **47**, RS2015 (2012).
10. R. E. Collin, *Field Theory of Guided Waves* (Wiley-IEEE, 1960).
11. A. D. Rakić, A. B. Djurišić, J. M. Elazar, and M. L. Majewski, "Optical properties of metallic films for vertical-cavity optoelectronic devices," *Appl. Opt.* **37**(22), 5271–5283 (1998).
12. A. D. Rakić, "Algorithm for the determination of intrinsic optical constants of metal films: application to aluminum," *Appl. Opt.* **34**(22), 4755–4767 (1995).
13. A. A. Goyadinov and V. A. Markel, "From slow to superluminal propagation: Dispersive properties of surface plasmon polaritons in linear chains of metallic nanospheroids," *Phys. Rev. B* **78**(3), 035403 (2008).
14. A. Rusina, M. Durach, and M. I. Stockman, "Theory of spoof plasmons in real metals," *Appl. Phys. A* **2**(2), 375–378 (2010).
15. P. Berini, "Long-range surface plasmon polaritons," *Adv. Opt. Photonics* **1**(3), 484–588 (2009).
16. D. Sarid, "Long-Range Surface-Plasma Waves on Very Thin Metal Films," *Phys. Rev. Lett.* **47**(26), 1927–1930 (1981).

17. F. Yang, J. R. Sambles, and G. W. Bradberry, "Long-range surface modes supported by thin films," *Phys. Rev. B Condens. Matter* **44**(11), 5855–5872 (1991).
18. M. Quinten, A. Leitner, J. R. Krenn, and F. R. Aussenegg, "Electromagnetic energy transport via linear chains of silver nanoparticles," *Opt. Lett.* **23**(17), 1331–1333 (1998).
19. W. H. Weber and G. W. Ford, "Propagation of optical excitations by dipolar interactions in metal nanoparticle chains," *Phys. Rev. B* **70**(12), 125429 (2004).
20. A. F. Koenderink and A. Polman, "Complex response and polariton-like dispersion splitting in periodic metal nanoparticle chains," *Phys. Rev. B* **74**(3), 033402 (2006).
21. J. R. Krenn, "Nanoparticle waveguides: Watching energy transfer," *Nat. Mater.* **2**(4), 210–211 (2003).
22. K. H. Fung and C. T. Chan, "Plasmonic modes in periodic metal nanoparticle chains: a direct dynamic eigenmode analysis," *Opt. Lett.* **32**(8), 973–975 (2007).
23. B. Willingham and S. Link, "Energy transport in metal nanoparticle chains via sub-radiant plasmon modes," *Opt. Express* **19**(7), 6450–6461 (2011).
24. D. G. Baranov, A. P. Vinogradov, and A. A. Lisyansky, "Magneto-optics enhancement with gain-assisted plasmonic subdiffraction chains," *J. Opt. Soc. Am. B* **32**(2), 281–289 (2015).
25. M. L. Brongersma, J. W. Hartman, and H. A. Atwater, "Electromagnetic energy transfer and switching in nanoparticle chain arrays below the diffraction limit," *Phys. Rev. B* **62**(24), R16356 (2000).
26. C. F. Bohren and D. R. Huffman, *Absorption and Scattering of Light by Small Particles* (Wiley, 2008).
27. P. R. West, S. Ishii, G. V. Naik, N. K. Emani, V. M. Shalaev, and A. Boltasseva, "Searching for better plasmonic materials," *Laser Photonics Rev.* **4**(6), 795–808 (2010).
28. G. V. Naik, V. M. Shalaev, and A. Boltasseva, "Alternative Plasmonic Materials: Beyond Gold and Silver," *Adv. Mater.* **25**(24), 3264–3294 (2013).
29. M. W. Knight, N. S. King, L. Liu, H. O. Everitt, P. Nordlander, and N. J. Halas, "Aluminum for plasmonics," *ACS Nano* **8**(1), 834–840 (2014).
30. D. Shah, H. Reddy, N. Kinsey, V. M. Shalaev, and A. Boltasseva, "Optical Properties of Plasmonic Ultrathin TiN Films," *Adv. Opt. Mater.* **5**(13), 1700065 (2017).
31. D. O. Sigle, E. Perkins, J. J. Baumberg, and S. Mahajan, "Reproducible deep-UV SERRS on aluminum nanovoids," *J. Phys. Chem. Lett.* **4**(9), 1449–1452 (2013).
32. L. Zhou, C. Zhang, M. J. McClain, A. Manjavacas, C. M. Krauter, S. Tian, F. Berg, H. O. Everitt, E. A. Carter, P. Nordlander, and N. J. Halas, "Aluminum nanocrystals as a plasmonic photocatalyst for hydrogen dissociation," *Nano Lett.* **16**(2), 1478–1484 (2016).
33. X. Jiao, E. M. Peterson, J. M. Harris, and S. Blair, "UV fluorescence lifetime modification by aluminum nanoapertures," *ACS Photonics* **1**(12), 1270–1277 (2014).
34. Y. Yang, J. M. Callahan, T.-H. Kim, A. S. Brown, and H. O. Everitt, "Ultraviolet nanoplasmonics: a demonstration of surface-enhanced Raman spectroscopy, fluorescence, and photodegradation using gallium nanoparticles," *Nano Lett.* **13**(6), 2837–2841 (2013).
35. J. B. Pendry, L. Martín-Moreno, and F. J. Garcia-Vidal, "Mimicking surface plasmons with structured surfaces," *Science* **305**(5685), 847–848 (2004).
36. F. Garcia-Vidal, L. Martín-Moreno, and J. Pendry, "Surfaces with holes in them: new plasmonic metamaterials," *J. Opt. A, Pure Appl. Opt.* **7**(2), S97–S101 (2005).
37. A. P. Hibbins, B. R. Evans, and J. R. Sambles, "Experimental verification of designer surface plasmons," *Science* **308**(5722), 670–672 (2005).
38. E. Kretschmann, T. L. Ferrell, and J. C. Ashley, "Splitting of the Dispersion Relation of Surface Plasmons on a Rough Surface," *Phys. Rev. Lett.* **42**(19), 1312–1314 (1979).
39. J. Chandezon, M. T. Dupuis, G. Cornet, and D. Maystre, "Multicoated gratings: a differential formalism applicable in the entire optical region," *J. Opt. Soc. Am.* **72**(7), 839–846 (1982).
40. M. E. Inchaussandague and R. A. Depine, "Parametric coordinate transformations for surface relief gratings," in *IV Iberoamerican Meeting of Optics and the VII Latin American Meeting of Optics, Lasers and Their Applications* (SPIE, 2001), p. 4.
41. T. C. Paulick, "Applicability of the Rayleigh hypothesis to real materials," *Phys. Rev. B Condens. Matter* **42**(5), 2801–2824 (1990).
42. P. M. van den Berg and J. T. Fokkema, "The Rayleigh hypothesis in the theory of reflection by a grating," *J. Opt. Soc. Am.* **69**(1), 27–31 (1979).
43. A. Yariv and P. Yeh, *Optical Waves in Crystals* (Wiley, 1984).
44. A. P. Vinogradov and A. V. Dorofeenko, "Near-field Bloch waves in photonic crystals," *J. Commun. Technol. Electron.* **50**, 1153–1158 (2005).
45. M. G. Blaber, M. D. Arnold, and M. J. Ford, "Search for the Ideal Plasmonic Nanoshell: The Effects of Surface Scattering and Alternatives to Gold and Silver," *J. Phys. Chem. C* **113**(8), 3041–3045 (2009).
46. T. V. Shahbazyan and M. I. Stockman, *Plasmonics: Theory and Applications* (Springer, 2013).
47. P. Sheng, *Introduction to Wave Scattering, Localization and Mesoscopic Phenomena* (Springer, 2006).
48. J. A. Nelder and R. Mead, "A simplex method for function minimization," *Comput. J.* **7**(4), 308–313 (1965).
49. A. A. Maradudin and W. M. Visscher, "Electrostatic and electromagnetic surface shape resonances," *Z. Phys. B* **60**(2-4), 215–230 (1985).
50. P. C. Das and J. I. Gersten, "Surface shape resonances," *Phys. Rev. B* **25**(10), 6281–6290 (1982).

51. A. V. Zayats, I. I. Smolyaninov, and A. A. Maradudin, "Nano-optics of surface plasmon polaritons," *Phys. Rep.* **408**(3-4), 131–314 (2005).
 52. C. F. Bohren and D. R. Huffman, *Absorption and Scattering of Light by Small Particles* (Wiley, 2008).

1. Introduction

Our appetite for higher-speed devices inevitably leads to the transition from electronic or optoelectronic to all-optical devices. At the same time, the necessity for higher clock frequencies for information processing requires greater integration of photonic devices and scaling them down to nanometers. In optics, dielectric fiber replaces the coaxial and strip transmission lines. However, the characteristic transverse size of a fiber line is orders of magnitude larger than the characteristic size of components of semiconductor integrated circuitry. Moreover, the radius of curvature for optical line bending reaches a few microns [1]. The resulting large total size of the device hinders the realization of a high clock frequency which is limited by the signal propagation time within the device. A possible solution for this problem is a transition from photons to surface plasmon-polaritons (SPPs).

The SPP is an electromagnetic wave propagating along the interface between a metal and dielectric. Our focus is on a possibility of the information transfer by SPPs. We, therefore, consider a situation close to an experiment: a source of the electromagnetic field with the frequency ω_0 is positioned at some point x_0 , and we are looking at the transmission line response at a distance Δx from the source. In this setting, the frequency is real, and the wave vector k_{SPP} has an imaginary part, which is responsible for the attenuation. Such a setting is typical for plasmonics [2–7]. Note that usually the wave vector is considered as a function of the frequency. In our study, an SPP is an eigensolution characterized by the complex propagation constant k_{SPP} and the real frequency ω [8, 9]. k_{SPP} is the wave vector component that is parallel to the direction of propagation of the SPP. It is related the transverse component via the dispersion law $k_{SPP}^2 + k_{\perp}^2 = \varepsilon_d (2\pi / \lambda_0)^2$, where λ_0 is the wavelength of light in vacuum. The wavelength of an SPP, $\lambda_{SPP} = 2\pi / \text{Re} k_{SPP}$, is smaller than that of the electromagnetic wave in the dielectric with permittivity ε_d , $\lambda_0 / \sqrt{\varepsilon_d}$. In case of no attenuation, $k_{\perp} = \sqrt{\varepsilon_d k_0^2 - k_{SPP}^2}$ is purely imaginary. The SPP is therefore confined to the metal surface with the transverse (perpendicular to the surface) confinement length

$$\delta = \frac{1}{\text{Im}(k_{\perp})} = \frac{\lambda_0 \lambda_{SPP}}{2\pi (\lambda_0^2 - \varepsilon_d \lambda_{SPP}^2)^{1/2}} \quad (1)$$

In the absence of losses, the SPP propagation length, $l_{pr} = 1 / (2 \text{Im} k_{SPP})$, would be infinite and both λ_{SPP} and δ would tend to zero as $\varepsilon_m(\omega)$ tends to $-\varepsilon_d$. For $\lambda_{SPP} \ll \lambda_0$, the confinement length is $\delta \approx \lambda_{SPP} / 2\pi \ll \lambda_0$. This enables the miniaturization of optical devices and the transition from electronics to on-chip plasmonics technology possible [2–7].

The main obstacle to the use of SPPs in applications is Joule losses in the metal. This substantially decreases the SPP propagation length, l_{pr} and also raises the SPP minimum wavelength, λ_{SPP}^{\min} . SPPs with λ_{SPP} smaller than λ_{SPP}^{\min} cannot exist [2]. This weakens the transverse confinement of the SPP.

The values of l_{pr} , λ_{SPP}^{\min} , and δ are strongly determined by the geometrical configuration. The dispersion curves $k_x(\omega)$ and parametric dependencies of $\delta(\omega)$ as a function of $l_{pr}(\omega)$ for various configurations are shown in Figs. 1(a) and 1(b), respectively. The curves in these figures are characterized in Table 1. In the terminal points A_i and B_i , the dispersion curves

cross the light cone or reach the plasma frequency. Points A_i and B_i denote upper lower bounds of the respective frequency range. In the low-frequency part of the spectrum, the SPP propagation lengths increase and B_i may absent. Consequently, in Figs. 1(b), the movement along the parametric curve $\delta(l_{pr})$ starting from points A_i corresponds to a decrease in the frequency.

Inside the light cone, the SPPs become the Zenneck waves [10]. Due to the small propagation length of these waves, we only consider the part of the dispersion curve outside the light cone.

In the simplest geometrical configuration of an SPP propagating along the flat interface between half-spaces filled by the metal and dielectric, the wavenumber of the SPP is given by [2]

$$k_{SPP} = k_0 \sqrt{\varepsilon_m \varepsilon_d / (\varepsilon_m + \varepsilon_d)}, \quad (2)$$

where k_0 is the free space wavenumber [2]. Due to loss in the metal, according to Eq. (2), the dependence $k_{SPP}(\omega)$ is not monotonic. At the first part of the curve $A_1 B_1$, the wavelength of SPP, λ_{SPP} , and the transverse confinement length, $\delta(\omega)$, decrease with a decrease in the frequency until $\lambda_{SPP}(\omega)$ and $\delta(\omega)$ reach the minimum values λ_{SPP}^{min} and δ_{min} , respectively. With a further decrease in the frequency, the $\lambda_{SPP}(\omega)$ and $\delta(\omega)$ increase (see Figs. 1(a) and 1(b), curves 1).

The minimum wavelengths for silver-vacuum and gold-vacuum interfaces are $\lambda_{SPP}^{min} \approx 0.78\lambda_0$ and $\lambda_{SPP}^{min} \approx 0.91\lambda_0$, respectively. Minimal transverse confinement lengths of SPPs in silver and gold are about $0.2\lambda_0$ and $0.36\lambda_0$, respectively. Unfortunately, at the maximal confinement ($\delta = \delta_{min}$), an SPP cannot propagate at all since $l_{pr}^{min} < \lambda_{SPP}^{min}$ (see Fig. 1(b), curve 1). At low frequencies ($|\hbar\omega| < 3.0\text{ eV}$), the SPP wavelength is of the order of the wavelength in the dielectric ($\lambda_{SPP} \approx \lambda_0 / \sqrt{\varepsilon_d}$) and the transverse confinement length is much greater than λ_{SPP} .

The propagation length may be increased, even to hundreds of wavelengths, by using thin metal films [15]. The corresponding dispersion curve for long-range SPPs is determined by the equation [2]

$$i \tan\left(\sqrt{\varepsilon_m k_0^2 - k_{SPP}^2} \frac{h}{2}\right) = \frac{\sqrt{\varepsilon_d k_0^2 - k_{SPP}^2} \varepsilon_m}{\sqrt{\varepsilon_m k_0^2 - k_{SPP}^2} \varepsilon_d}, \quad (3)$$

where h is the thickness of the metal film. According to Eq. (3), the dispersion curve of the long-range SPP is close to the light cone (see Fig. 1(a), curve 2), so its wavelength λ_{SPP} is about λ_0 , while the confinement length tends towards infinity [15–17]. In other words, the SPP tends to a plane wave, and the plasmonic thin films turn into an analog of a single-wire transmittance line (see curve 2 in Figs. 1(a), (b)). At the point A_2 , curve 2 ends crossing the line cone. Such a transmittance line has no advantages compared to a common optical dielectric waveguide.

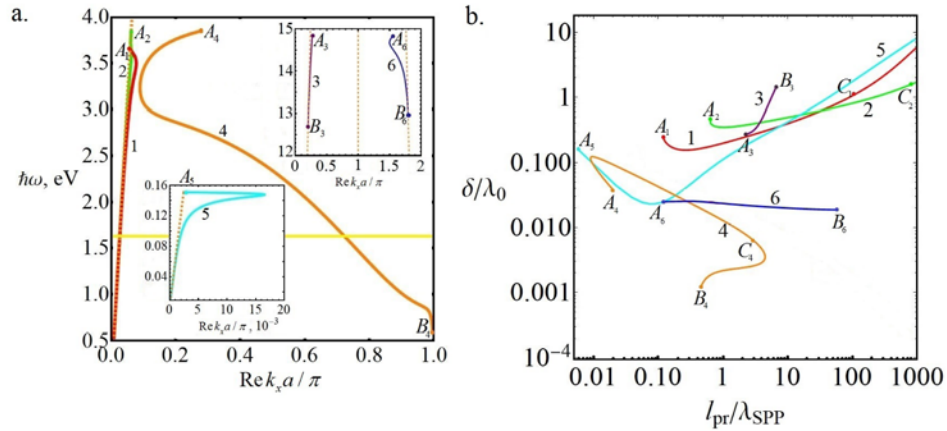


Fig. 1. The dispersion curves (a) and the parametric dependence of the transverse confinement length $\delta(\omega)$ on the propagation length $l_{pr}(\omega)$ (b) for different topologies that support SPPs. In insets of Fig. 1(a), the frequency units are eV. For details, see Table 1. In Fig. 1(b), points C_i correspond to the boundary of the visible and IR regions assumed to be 780 nm (1.6 eV); in Fig. 1(a), this boundary is shown by the yellow line; segments $A_i C_i$ correspond to the visible region. In the manuscript, for numerical calculations, we assume that the dielectric is vacuum with $\epsilon_d = 1$.

Table 1. The dependencies $k_x(\omega)$ and $\delta(l_{pr})$ for various transmission lines. For dielectric permittivities of aluminum and silver, the data from Refs [11], and [12] were used.

Curve # (color)	Transmission line	A_i (upper bound of the frequency region)	B_i (lower bound of the frequency region)
1 (red)	Flat surface silver half-space	DCILC ^a	Does not exist
2 (green)	30-nm-thin silver film (long-range SPP)	DCILC	Does not exist
3 (purple)	Chain of oblate aluminum spheroids (longitudinally polarized mode) [13]	Plasma frequency	DCILC
4 (orange)	Chain of oblate silver spheroids (transversely polarized mode)	DCILC	Does not exist
5 (cyan)	Microstructured silver surface (Spoof SPP) [14]	DCILC	Does not exist
6 (blue)	Nanostructured aluminum surface	Plasma frequency	DCILC

^aDCILC - dispersion curve intersection with the light cone

Using chains of metal nanoparticles allows one to decrease both the wavelength of an SPP and its transverse confinement length [13, 18–25]. In the quasistatic approximation, in which only the nearest neighbor interaction is taken into account, the dispersion law of nanoparticles periodically positioned along the chain is either [24, 25]

$$k_{SPP} = \frac{1}{a} \arccos \left[\frac{a^3}{4\alpha(\omega)} \right], \quad (4)$$

for dipole moments parallel to the direction of propagation (the longitudinal polarization), or

$$k_{SPP} = \frac{1}{a} \arccos \left[-\frac{a^3}{2\alpha(\omega)} \right], \quad (5)$$

for dipole moments perpendicular to the direction of propagation (the transverse polarization). In Eqs. (4) and (5), the nanoparticles are considered as point dipoles and $\alpha(\omega)$ is the polarizability of a nanoparticle [26]. In [13], Eqs. (4) and (5) are generalized by including retardation effects. For oblate spheroids, the propagation length exceeding a hundred of λ_{SPP} is predicted. Such a great $l_{pr}(\omega)$ requires a large ratio of the greatest axis of the spheroid to the distance between spheroids. Our evaluations show that approximating nanoparticle by point dipoles results in a substantially overestimated $l_{pr}(\omega)$. Note, that unless we are working far from the stop band, the effects of retardation are not important. Neglecting the retardation effects and taking into account size effects results in curves 4 (Fig. 1) showing the propagation length smaller than a dozen of λ_{SPP} .

In contrast to the transverse SPP mode, the mode with the longitudinal polarization (see Fig. 1, curves 3) exists in the ultraviolet part of the spectrum in which $-\epsilon_d < \text{Re } \epsilon_m(\omega) < 0$. In gold and silver, this mode is non-existent due to high losses caused by inter-band transitions. Thus, in the visible region, even the best plasmonic materials, such as gold and silver, are not suitable for applications that require $\delta \ll \lambda_0$ and l_{pr} of the order of a dozen SPP wavelengths.

The search for new plasmonic materials has been growing sharply in recent years [27–30]. In particular, the transition to the ultraviolet part of the spectrum brings into consideration new materials, such as aluminum [29, 31]. The mode with the longitudinal polarization can propagate in chains of oblate aluminum nanospheroids (see curves 3 in Fig. 1). The upper bound of the narrow region in which this mode can propagate is the plasma frequency. Therefore, the SPP frequency is close to the plasmon resonance of the nanoparticle. This leads to large losses so that the propagation length of an SPP is only a few λ_{SPP} (in Fig. 1, curves 3 originate at the points A_3 at which the dispersion curve crosses the light cone and ends at the point B_3 at which the real part of the metal permittivity becomes positive). Short propagation lengths of both transverse and longitudinal modes substantially limit their practical use.

Using aluminum allows for significant enhancements of UV fluorescence and the rates of photochemical reactions [31–34]. In Sections II-IV, using aluminum as an example, we consider the propagation of strongly localized SPPs. The effects under consideration cannot be observed in silver and gold. It would also be highly desirable to obtain topologically more complicated interfaces that combine advantages of the aforementioned systems without their shortcomings.

In this paper, we demonstrate that a periodically nanostructured metal-dielectric interface (an array of metal nanoparticles deposited on the metal surface) supports an SPP mode which transverse confinement length and the wavelength are comparable to the period of the structure. In contrast to spoof SPPs that exist on structured surfaces in the far-infrared region [14, 35–37], the eigenfrequency of the suggested mode is in the ultraviolet part of the spectrum (λ is in the range from 83 to 115 nm). This mode cannot be observed in traditional plasmonic materials due to high losses caused by interband transitions in this part of the spectrum. In the ultraviolet region, losses in aluminum are relatively small because interband transitions are in the visible region. Therefore, the propagation length of the SPP can be as large as several dozens of λ_{SPP} on a periodically nanostructured aluminum-dielectric interface.

2. Nanostructured surface

In the absence of losses, on a rough metal surface, an additional SPP may arise [38]. The solution corresponding to this SPP has been obtained with the assumption that for a smooth

surface, near the frequency for which $\varepsilon_m(\omega) = -\varepsilon_d$, the group velocity of the SPP is zero. This provides a resonance interaction of the field with all harmonics of the roughness. As a result, the frequency curve splits and the second SPP mode with large k arises. However, in a lossy system, on a smooth surface, an SPP with sufficiently large wavenumbers does not exist. In addition, the assumption of zero group velocity, which is necessary for the second branch of the SPP, is not realistic. Therefore, it is not clear whether in a lossy system an additional SPP may arise.

To model periodically nanostructured metal-dielectric interface, we consider a system shown in Fig. 2. The interface between the metal and dielectric is modulated by the function $s(x) = h \cos(2\pi x/a)$. The upper half-space is a dielectric with the permittivity ε_d and the lower half-space is a metal with the permittivity ε_m . We look for a frequency-domain solution as a TM-polarized wave propagating along the x -axis. Since the roughness is periodic, we seek for the solution in the form $H_y = F(x, z)e^{ik_x x}$, where H_y is the magnetic field strength of the SPP, $F(x, z)$ is periodic in the x -direction function with the period a , and $k_x = k'_x + ik''_x$ is the propagation constant.

To solve Maxwell's equations, we use the coordinate transformation [39, 40] which makes the interface flat, but coefficients in the equations become periodic with respect to x . This method is even applicable for a large amplitude of roughness when the Rayleigh hypothesis is invalid [41, 42]. Within the framework of this method, the tangential components of the electric and magnetic fields are represented as a series of Bloch harmonics. This allows one to reduce Maxwell's equations to the system of linear differential equations with constant coefficients and to obtain expressions for the fields in both media analytically. By using the Maxwell boundary conditions, one can obtain the propagation constant $k_x(\omega)$ of the eigensolution as a function of frequency.

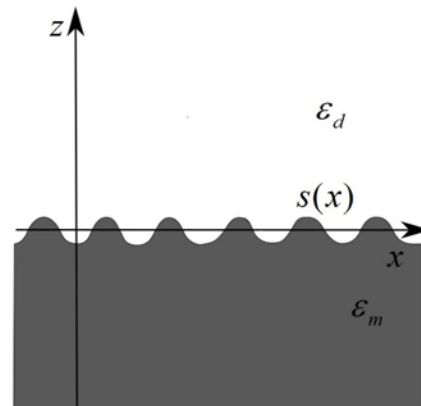


Fig. 2. The schematics of the system studied.

3. Analysis of the dispersion curves for the nanostructured surface

For an SPP, a periodically nanostructured surface is a photonic crystal. For typical plasmonic materials such as silver and gold, the SPP curve in the second Brillouin zone cannot be observed due to high losses in the UV frequency region in which these losses are due to the interband transitions. In the UV part of the spectrum of aluminum, losses are small because interband transitions are in the visible part of the spectrum. Therefore, in aluminum, this SPP dispersion branch can be observed.

First, we consider a hypothetical lossless vacuum-aluminum system. The dispersion functions, $k_x(\omega)$, of SPPs on the nanostructured surface for various amplitudes of the

interface profile are shown in Fig. 3. The dispersion curve (shown by the blue line in Fig. 3) $k_x(\omega)$ of the SPP propagating on the flat surface ($h=0$) is described by Eq. (1) [2]. For small h , similar to photonic crystals, due to the Bragg reflection of plasmon-polaritons between neighboring surface inhomogeneities, the band gap at $k_x a / \pi = 1$ opens up (the red line). The width of this band gap increases with an increase of h [43]. At a certain value of h , in the second Brillouin zone, a part of the dispersion curve moves to the frequency region, in which $\text{Re} \varepsilon_m(\omega) > -\varepsilon_d$. In this region, SPPs on a flat metal-vacuum interface do not exist because k_x becomes pure imaginary. One might expect that the “plasmon” band gap should arise in this region. However, there is a passband because, in a periodic system, the energy can be transferred by evanescent fields [44].

In a lossless system, the dispersion curves for interfaces with technologically achievable amplitudes of the surface perturbation ($h=5$ nm and $a=10$ nm in our calculations) are shown in Fig. 4(a). In this case, the band gap arises for the wavelengths 97 nm – 207 nm. In the first Brillouin zone, the dispersion curve of the SPP becomes non-monotonic, and a point in which the group velocity is zero arises. In the second Brillouin zone, the dispersion curve moves completely to the frequency region defined by the inequality $\text{Re} \varepsilon_m(\omega) > -\varepsilon_d$. In this zone, the waves are backward.

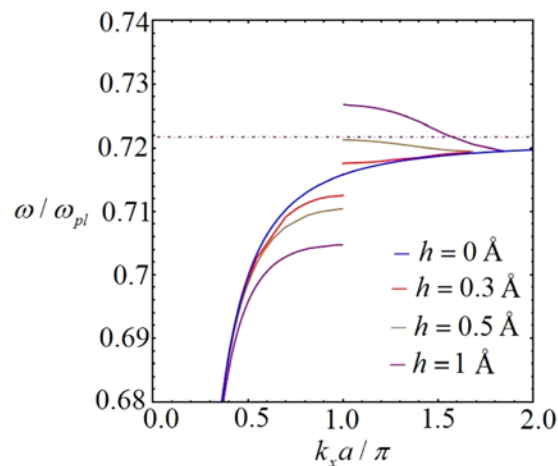


Fig. 3. The dispersion curves of the SPP on the nanostructured surface for various modulation amplitudes h . The period of the modulation is 10 nm. The dielectric permittivity of metal assumed to be equal to the permittivity of aluminum taken from Ref [12]. The dash-dotted purple line corresponds to $\omega / \omega_{pl} = 0.73$ at which $\text{Re} \varepsilon_m = -\varepsilon_d$ (ω_{pl} is the plasma frequency).

Losses change the SPP dispersion curves significantly [see curve 6 in Figs. 1(a), 1(b) and 4(b)]. One can see that in the first Brillouin zone, $k_x a / \pi < 1$, at the point in which in the absence of loss, the group velocity is zero, the SPP curve splits into two branches. Both of these branches are in the visible region. One of the branches has a negative slope corresponding to the backward wave. Because the respective wavenumber is of the order of $\pi / 2a$ [see Fig. 4(b)], this wave exists far from the light cone where it may be strongly confined. However, computer simulations show that on an aluminum surface, the propagation length of the SPP associated with this curve is small. It is not more than the SPP wavelength. Even for silver, which in visible does not have interband transitions, the propagation length does not exceed the SPP wavelength.

For a and h of the order of 10 nm, the attenuation may depend on the surface inhomogeneities because their size becomes comparable with the electron mean free path in metal [45]. For silver and gold, the electron mean free path is 20-30 nm [45, 46]. In aluminum, the electron mean free path is 2 nm [45]. Therefore, in aluminum, the electron scattering off the surface is small, and there is no additional loss due to the smallness of the structure. Thus, to calculate the SPP dispersion branch in the second Brillouin zone, one may use bulk values for aluminum permittivity.

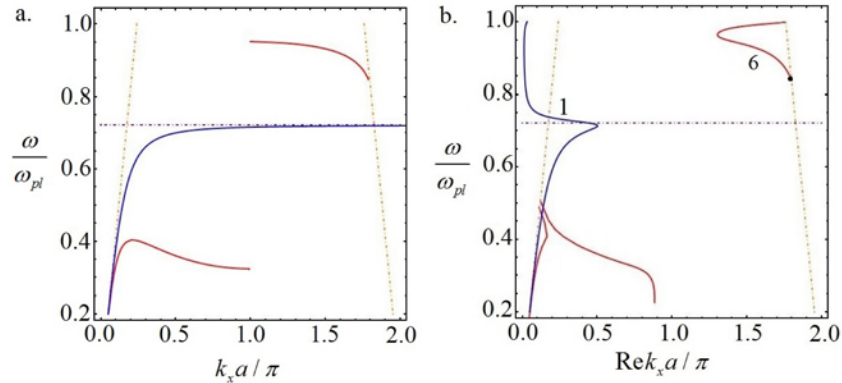


Fig. 4. The dispersion curves of the SPP on an aluminum surface calculated without (a) and with (b) taking loss into account. The dispersion curve of the SPP on flat and nanostructured surfaces are shown by blue and red lines, respectively. The structure parameters are $h = 5$ nm and $a = 10$ nm. Orange lines show boundaries of the light cone, the dash-dotted purple line corresponds to $\omega / \omega_{pl} = 0.73$. $\text{Re}\epsilon_m = -\epsilon_d$ for the frequency $\omega = 0.73\omega_{pl}$. In this figure, the line numbering is the same as in Fig. 1.

Since the SPP dispersion curve 6 in Fig. 4(b) is in the second Brillouin zone, the wavelength of the SPP should be determined by the period of the surface structure. Indeed, this wavelength is related to the propagation constant $k_x \approx 2\pi/a$ as

$$\lambda_{SPP} = \frac{2\pi}{\text{Re}k_x} \approx a. \quad (6)$$

The smallness of the SPP wavelength implies the subwavelength confinement of the SPP. Indeed, numerical calculations presented in Fig. 5 show that the field intensity is mainly confined near the surface. Since the frequency of the SPP is equal to the light frequency in a vacuum, it is clear that the field of the SPP is confined on a subwavelength scale.

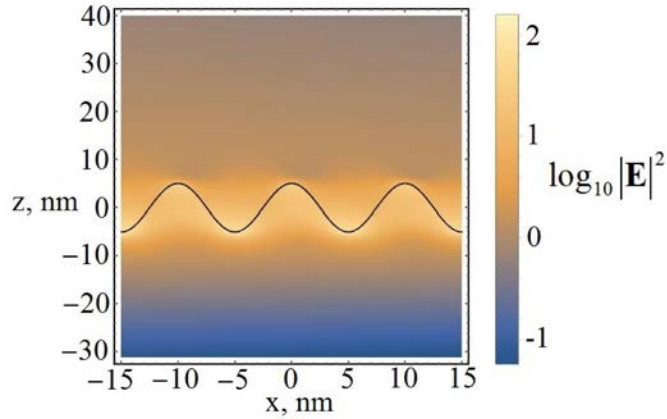


Fig. 5. The distribution of the electric field intensity $|\mathbf{E}|^2$ near the interface. The values of ω and k_x used in numerical calculations are marked by the black point in Fig. 4(b).

Note that in the second Brillouin zone, a strongly confined SPP with the Bloch wavenumber $k_x = k_{Bl}$ also includes the harmonic with the wavenumber $k_x = k_{Bl} - 2\pi/a$, that belongs to the first Brillouin zone. Though we consider $(k_{Bl} - 2\pi/a) > k_0\sqrt{\epsilon_d}$, the difference between $k_{Bl} - 2\pi/a$ and $k_0\sqrt{\epsilon_d}$ is small and the corresponding harmonic has weak transverse confinement. Nevertheless, the amplitude of this harmonics is much smaller than that of the Bloch harmonics corresponding to the second Brillouin zone [47]. This is confirmed by our computer simulation. As a result, the Bloch harmonics of the first Brillouin zone does not affect much the confinement of the SPP.

The strongly confined SPP propagates over relatively long distances. Its propagation length l_{pr} can be determined by the equation

$$\frac{l_{pr}}{\lambda_{SPP}} = \frac{\text{Re}k_x}{4\pi\text{Im}k_x}, \quad (7)$$

where l_{pr} is defined as the distance over which the field intensity decreases by the factor of e . On the sine surface with the amplitude of 5 nm, the maximum value of the SPP propagation length is about 17 SPP wavelengths. By optimizing the surface structure, one can increase this length significantly. By using the Nelder–Mead method for optimization [48], we find that the optimal surface profile is given parametrically by the equations:

$$\begin{aligned} z(v) &= h \cdot 2^{-0.838(v/\gamma)^4} \left[1 + 0.075 \left(2^{-14.65(v-a/3)^2/\gamma^2} + 2^{-14.65(v+a/3)^2/\gamma^2} \right) - 0.52 \cdot 2^{-0.003(v/\gamma)^4} (v/\gamma)^2 \right], \\ x(v) &= v \left[0.996 + 0.024 \left(e^{-10.17(v-0.13a)^2/\gamma^2} + e^{-10.17(v+0.13a)^2/\gamma^2} \right) \right. \\ &\quad \left. - 0.16 \left(e^{-10.17(v-0.26a)^2/\gamma^2} + e^{-10.17(v+0.26a)^2/\gamma^2} + e^{-10.17(v-0.35a)^2/\gamma^2} + e^{-10.17(v+0.35a)^2/\gamma^2} \right) \right. \\ &\quad \left. - 0.29(v/\gamma)^2 \left(e^{-4(v-0.083a)^2/\gamma^2} + e^{-4(v+0.083a)^2/\gamma^2} \right) \right], \end{aligned} \quad (8)$$

where the height of modulation is $h = 18.5$ nm, the period is $a = 10$ nm, $\gamma = 2.5$ nm, and v is the parameter varying in the range from $-a/2$ to $a/2$. The profile of the surface is shown

in Fig. 6. With the surface profile given by Eq. (7), the SPP propagation length is about $53\lambda_{SPP}$ or 628 nm. Its frequency dependence is shown in Fig. 7.

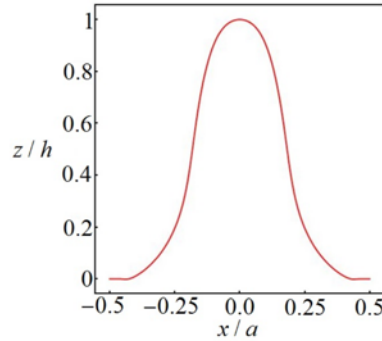


Fig. 6. The optimal surface structure defined by Eq. (6).

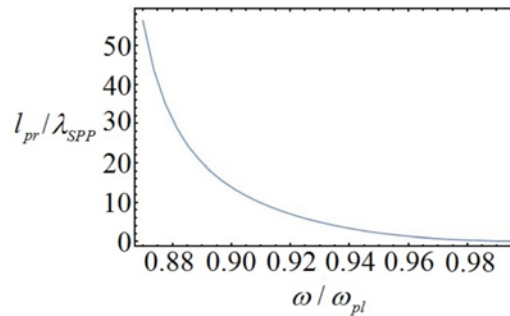


Fig. 7. The dependence of the SPP propagation length on its frequency on the optimized nanostructured interface.

The profile given by Eq. (8) may be difficult to realize experimentally. However, our numerical simulations demonstrate that the effect reported in the paper is fairly stable to variations of the surface profile.

4. Mechanism for the formation of the strongly confined SPP

To explain the formation of the strongly confined SPP, we represent the sine-profile of the surface,

$$s(x) = h \cos(2\pi x / a), \quad (9)$$

as a chain of peaks with the height $2h$ and the width $a/2$, spaced by the distance a . Electric charge accumulates on inhomogeneities with a small radius of curvature increasing the electric field strength near the spike [6]. Spikes, therefore, have high polarizabilities. In addition, the high polarizability of a spike can arise due to localized plasmon resonances [49–51]. If spikes have the same shape and are located close to each other, then a propagating mode arises [24].

Assuming that the chain of spikes is equivalent to the chain of two-dimensional dipoles with the polarizability $\alpha(\omega)$, one can obtain the dispersion law for the propagating mode. Numerical calculations show that a dipole moment of a spike is directed along the SPP propagation direction, x . Therefore, we consider the longitudinally polarized mode of the dipole chain. The dipole moment of the i -th spike is determined by the equation:

$$d_i = \alpha(\omega) \sum_{n \neq i} E_{x,n}(x_i), \quad (10)$$

where $E_{x,n}(x_i)$ is the electric field of the n -th dipole acting on the i -th dipole. It can be determined by using the equation:

$$E_{x,n}(x) = d_n \left(\frac{d^2}{dx^2} + k_0^2 \right) G(x, x_n), \quad (11)$$

where $G(x, x_i) = i\pi H_0^{(1)}(k_0 |x - x_i|)$ is the Green function of the two-dimensional Helmholtz equation. Since the chain is periodic, the dipole moments of spikes are related via the Bloch theorem:

$$d_n = d_i e^{ik_x(n-i)a}. \quad (12)$$

Excluding d_i from Eqs. (10) and (11) we obtain the dispersion law:

$$1 = 2i\pi\alpha(\omega) \sum_{n=1}^{\infty} \left(\frac{d^2}{dx^2} + k_0^2 \right) H_0^{(1)}(x) \Big|_{x=nk_0a} \cos(nk_x a). \quad (13)$$

Let us assume that the polarization of a single peak, $\alpha(\omega)$, has the form [52]:

$$\alpha(\omega) = \alpha_m(\omega) \frac{1 - \varepsilon_{\max}}{\varepsilon_m(\omega) - \varepsilon_{\max}} bh, \quad (14)$$

where $\alpha_m(\omega) = (\varepsilon_m(\omega) - \varepsilon_d)(4\pi)^{-1}$ is the polarizability of a metal and ε_{\max} is the permittivity for which the polarizability reaches its maximum value. The dispersion curves calculated by using the coordinate transformation [39, 40] and with the help of Eqs. (13) and (14) are shown in Fig. 8. For calculations, we consider the lossless case and assume that $a = 10$ nm, $h = 5$ nm, and $\varepsilon_{\max} = -0.24\varepsilon_d$. We use such a value of ε_{\max} because as the distance between peaks increases, the dispersion curve calculated with the help of the method coordinate transformation becomes a straight line $\omega \approx \omega_{\max} = \text{const}$ at which $\varepsilon(\omega_{\max}) = \varepsilon_{\max} = -0.24\varepsilon_d$. Both curves are qualitatively the same: they have the same slopes and are approximately in the same frequency region. This shows that strongly confined SPP modes arise due to the high polarizability of surface inhomogeneities.

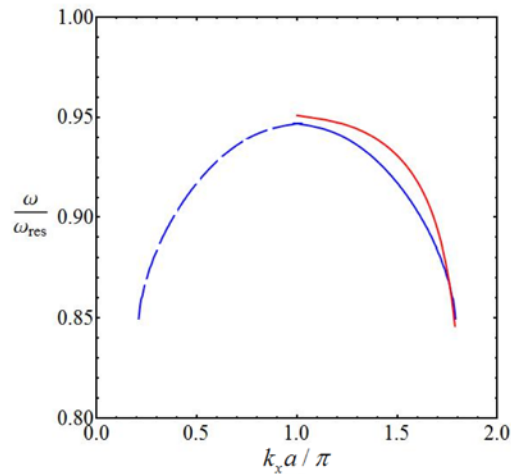


Fig. 8. The dispersion curves calculated by using the coordinate transformation [39, 40] (the red line) and with the help of Eqs. (13) and (14) (the blue line). The latter curve is extended to the second Brillouin zone.

5. Conclusion

In this paper, we have shown that strongly confined SPPs traveling dozens of wavelengths exist on a periodically nanostructured interface between a metal and dielectric. This mode, being a Bloch wave, exists near the second stop band. In contrast to Bloch waves in solids, an electromagnetic Bloch wave has a harmonic, which amplitude is much greater than all other harmonics of the wave. It is the wavenumber of this harmonic that determines the transverse confinement length of the wave. In the second passband, this wavenumber is about $2\pi/a$; therefore, its confinement length is $\delta \sim a/(2\pi)$. In our case, the second passband lies in the UV range where no SPPs are traveling along flat surfaces. Therefore, the Bloch wave is tunneling from one surface peak to another. This decreases the Joule losses consequently increasing the propagation length. A similar mechanism of an SPP propagation is realized for the longitudinally polarized mode in a chain of oblate nanospheroids [13]. Both modes are in the UV part of the spectrum. However, our computer simulation shows that the chain mode requires a greater dipole moment of a spheroid than the dipole moment of a peak on a nanostructured surface. As a result, the chain mode has a higher concentration of the electric field inside the ellipsoids. This results in greater losses leading to a smaller propagation length of this mode compared to the propagation length of an SPP along a nanostructured surface. In addition, the chain mode has a large confinement length because it exists in the first passband.

In traditional plasmonic materials, such as silver or gold, for ultraviolet frequencies, the SPP propagation length would be extremely small due to interband transitions. The suitable metal for the modes considered in the paper is aluminum in which losses are small in the ultraviolet region. In addition, the electron mean free path in these metals is about 2 nm providing small surface scattering. The period of the nanostructure, which may be 10-20 nm, determines the wavenumber of the SPP and results in strong confinement, which is crucial for SPP sensing and enhancement of nonlinear effects. Strong field localization also makes possible further miniaturization of a variety of “plasmonic optical” devices.

Funding.

National Science Foundation (NSF) (DMR-1312707).